Stamboroski *et al. Appl Adhes Sci (2016) 4:6*
DOI 10.1186/s40563-016-0063-7

Applied Adhesion Science

RESEARCH Open Access

Implementation of diverse non-centrosymmetric layer concepts for tuning the interface activity of a magnesium alloy

Stephani Stamboroski[1,2], Priscilla Natalli Stachera[1,3], Yendry Regina Corrales Ureña[1,4,5], Gustavo Homann Hrycyna[1,3], Wilson Iraja Taborda Ribas Neto[1,3], Wagner Kazuki de Azambuja[1,3], Dirk Salz[1], Jörg Ihde[1], Paul-Ludwig Michael Noeske[1*] and Welchy Leite Cavalcanti[1]

*Correspondence: Michael.Noeske@ifam.fraunhofer.de
[1] Department of Adhesive Bonding Technology and Surfaces, Fraunhofer Institute for Manufacturing Technology and Advanced Materials IFAM, Wiener Straße 12, 28359 Bremen, Germany
Full list of author information is available at the end of the article

Abstract

Magnesium and its alloys are the lightest metallic materials used for structural applications. Tuning the surface functionalization of magnesium alloys may contribute to increasing their durability. Dry or wet processes may be effective for the modification of magnesium alloy surfaces. The resulting layers may cover surface inhomogeneities and separate the substrate surface from molecular films. This work demonstrates the feasibility and effectiveness of the concepts and techniques comprising laser or plasma based pretreatment processes or dipping procedures that involve synthetic amphiphilic polymers or biopolymers. In detail, the effects of barrier layers that have been applied by the deposition of siliceous polymer coatings in low pressure plasma processes, by laser surface treatments in controlled gas atmospheres or by dipping in liquid formulations containing a recently developed polymeric inhibitor or a mixture of the enzyme laccase and the polysaccharide maltodextrin are monitored. In this respect, a time-resolved hydrogen bubble formation test is performed, revealing interactions between water films and the modified surfaces. The surface modification is shown with X-ray photoelectron spectroscopy investigations and, in addition, the alloy surface and grain structure is characterized using energy dispersive X-ray analysis, scanning electron microscopy and scanning force microscopy. These investigations reveal that the thus established layer/substrate and layer/environment interphases differ in their composition as a result of the non-centrosymmetric layer concepts for surface functionalization applied here.

Keywords: Magnesium aluminium alloy AM50, Functional surface layers, Laser surface treatment, Plasma polymer layer, Polymeric corrosion inhibitor, Laccase biopolymer functionalization, Polymeric interfactants, Surface analysis, Non-centrosymmetric surface layer concepts

Background

Due to their low density and adequate mechanical properties, magnesium and its alloys are promising materials for structural applications [1]. Their limited corrosion resistance [2] leads to their restricted use in technical applications but facilitates the design of biodegradable magnesium alloys [3, 4]. Considering that surface properties govern the

onset of material degradation, modifying the corrosion resistance of such alloys can be assessed by tailoring their surfaces or the respective interfaces in contact with the magnesium substrates. On the one hand, an elevated corrosion resistance is desired when heading for long-term adhesion-based applications, e.g. coating or adhesive bonding. On the other hand, a suitable corrosion rate in body fluids as well as a high biosafety is required for magnesium alloys in biomedical applications [5].

Often such surface modification is based on layer-forming approaches and the involved layers will have to feature a beneficial adhesion to the substrate as well as adequate cohesive properties. Additionally, they have an advantage in that they offer a functional base for further layers within a multilayer system or for exposure to the environment when constituting the terminal layer [6]. In adhesive bonding, multilayer systems may be aspired, as depicted in Fig. 1a for a lap-shear sample with two both identical and identically pretreated adherents. The layer system comprises the surface pretreatment layer and the primer layer on each adherent, e.g. a metal substrate, and, upon the application and compression of a cylindrical adhesive bead during the manufacture of the joint, a centrosymmetric multilayer system results. In contrast, open adhesive joints and especially painting or functional coatings [7] are typically not centrosymmetric multilayer systems, as shown in Fig. 1b.

The aim of this contribution is to substantiate that, within the scope of manufacturing functional coatings or adhesive joints, individual layers within the multilayer system may be advantageously designed to be non-centrosymmetric. Thus the particular interfaces and the resulting interphases around the layers can be functionalized individually and their interaction with neighboring layers can be tuned. Microscopically, the interphases—characterized by their chemical composition or conformational equilibria [8]—and the interactions undergo dynamic changes during the manufacture and application of the multilayer systems [9].

Concerning the surface functionalization processes addressed in this contribution, the molecular mass of the adsorptive species increases in sequence from a or b towards c or d, as shown in Fig. 2. Cases a and b represent the adsorption from a gas phase with volatile reactive species, while cases c and d represent the adsorption from a liquid phase containing polymeric molecules that have a vapor pressure too low for vapor deposition. The resulting dual layer may be perceived as a two-dimensional Janus system [10]. Likewise, the particulate polymeric species depicted as adsorbates in cases c or d may be perceived as anisotropic non-centrosymmetric nanoparticles and, in greater detail, as Janus particles (case c) or patchy particles (case d) [11]. We will investigate the concentration-dependent

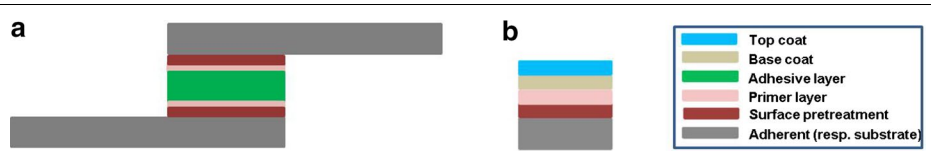

Fig. 1 Sketches of multilayer systems forming an adhesive joint of identical adherents in the geometry of a lap-shear test specimen (**a**), and a non-centrosymmetric coating system (**b**) on a substrate

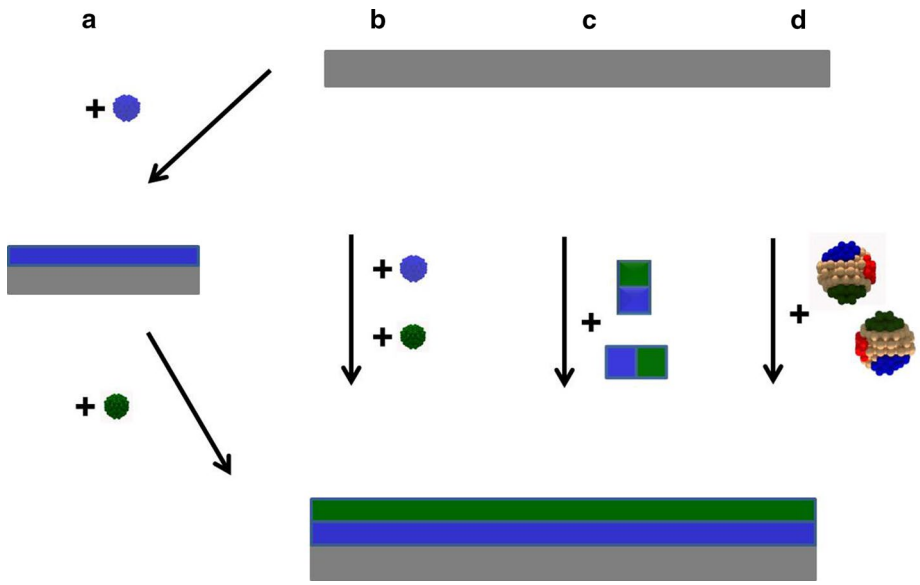

Fig. 2 Sketch showing the four different surface functionalization processes (**a**, **b**, **c**, and **d**) addressed in this contribution, resulting in dual layer coatings on a substrate. Details are given in the text

adsorption behavior of a synthetic amphiphilic polymer [12] and the interaction between a magnesium alloy substrate and an aqueous biopolymer mixture containing the nanoparticulate enzyme laccase, similar to the formulation recently described in an interaction with acidic silicon oxide surfaces [13]. Thin films containing biopolymers recently were tested with respect to improving the corrosion resistance of magnesium alloys [14, 15]. In cases a and b the non-centrosymmetric layer structure is achieved by scheduling the access of two molecularly different species to the respective substrate surface. Specifically, two reactive systems will be examined: one will use oxygen and hexamethyldisiloxane (case a) and a second will use oxygen and carbon dioxide (case b) as adsorptive species. The required activation energy will be provided by a plasma source [16, 17] and a laser source [18], respectively. Surface modification with thin films composed of organosilicon-based plasma polymers was reported to be a promising approach for the corrosion protection of magnesium alloys, e.g. using plasma enhanced chemical vapor deposition (PECVD) of superhydrophobic films from a mixture of trimethylmethoxysilane and argon [19], or atmospheric pressure PECVD from a mixture of tetraethoxysilane and oxygen [20]. Laser-based surface treatment of metal adherents was reported for titanium surfaces [21] and, more recently, for the magnesium alloy AZ31 [22].

Finally, the time-dependent interaction of molecular films applied to an AM50 magnesium alloy substrate was assessed using a liquid water film as a probe system for all the layer systems depicted in Fig. 2. In a previous contribution [12], the contact between water films and polished AM50 substrates was shown to result in the generation of hydrogen bubbles within three seconds. The effect of the investigated functional layers on the kinetics of the hydrogen bubble formation, as represented by the onset time and the area density of evolving bubbles, may reveal their performance in competing with water molecules for active adsorption sites on the magnesium alloy surfaces.

Methods

This section details the experimental procedures applied during the manufacture of the layer systems on AM50 alloy surfaces. Moreover, the analysis methods used for characterizing the layers and their effects on hydrogen bubble formation in contact with liquid water films will be described.

Experimental procedures

In order to create fresh surfaces under ambient conditions, samples of magnesium alloy AM50 (Rocholl GmbH, Aglasterhausen, Germany) were cut and manually polished using dry and flat SiC sandpaper with a grit size of 800 mesh.

Plasma polymeric coatings were applied to the surface of the pre-treated AM50 substrates using a low pressure plasma enhanced chemical vapor deposition (PECVD) technique. The home-built low pressure plasma chamber was equipped with a TRUMPF Hüttinger Quinto system for radio frequency (13.56 MHz) generation. Three different $SiO_xC_yH_z$–type coatings based on highly crosslinked plasma polymer primer layers were prepared with a variation in the deposition parameters, in particular regarding the mixing ratio between the gaseous educts hexamethyldisiloxane (HMDSO) and oxygen. This resulted in coatings with low, medium and high carbon concentrations, as revealed by X-ray photoelectron spectroscopy (XPS) investigations.

Furthermore, the AM50 surfaces were laser-treated in an O_2 and CO_2 containing gas atmosphere under ambient pressure. The laser treatment was performed on polished AM50 samples using a cleanLaser 250 system comprising a Q-switched Nd-YAG laser with a wavelength of 1064 nm. A pulse duration of 80 ns was applied.

A third approach was the use of the water-based formulation G50 wb of the amphiphilic polymer additive G50 (Straetmans High TAC GmbH, Hamburg, Germany), as described elsewhere [12]. Based on a parent formulation containing 1 wt% of organic constituents comprising polymer and triethanolamine (TEA) for adjusting the pH value, diluted formulations were prepared by adding demineralized water to the parent formulation.

Finally, a laccase mixture suspension (concentration 0.1 mg/ml) was prepared with laccase from a *Trametes versicolor*/maltodextrin powder mixture (from ASA Spezialenzyme GmbH, Wolfenbüttel, Germany) in water. The suspension was prepared at 25 °C using deionized water and working under aseptic conditions.

Analysis methods

Investigations into the surface composition were performed by X-ray photoelectron spectroscopy (XPS) applied to small pieces cut from the AM50 sheets. XPS spectra with an information depth of around 0.01 µm were taken using a Kratos Ultra system applying excitation of photoelectrons by monochromatic Al K_α radiation within an area of approximately 0.2 mm^2. The system was operated at a base pressure of 4×10^{-8} Pa and the sample neutralization was performed with low energy electrons (<5 eV). An electrostatic lens was used, the take-off angle of the electrons was 0°, and the pass energy was fixed to 20 eV (or 40 eV in the case of some of the less concentrated constituents) in high resolution spectra and 160 eV in survey spectra. Elemental ratios were calculated based

on the area of the peaks and considering relative sensitivity factors. The binding energy calibration of the electrically isolating samples was performed by referring the C 1s component of aliphatic carbon species to 285.0 eV. Binding energies are given with a precision of ±0.1 eV throughout this contribution.

An aerosol wetting test (AWT) was used to characterize the wetting properties of selected surfaces. In this test, monodisperse droplets of an aerosol are generated using an ultrasound nozzle and are applied to the substrate surface forming wide or narrow drops depending on the surface state and surface energy. In this manner, the wettability of surfaces can be characterized by evaluating the resulting droplet size distribution. Details of this technique are described elsewhere [12, 23].

The sample topography was studied using a scanning probe microscope (SPM) operated as a scanning force microscope in the 'tapping mode' in air (Digital Instruments Nanoscope III multimode). The maximum scan range of the scanner was 150 µm, and Si cantilevers (Nanosensors) with resonance frequencies of around 250 kHz corresponding to force constants of around 20 N/m were used. The nominal tip diameter was in the range of 10 nm.

The SEM examination of the samples was performed in a field emission scanning electron microscope (FESEM), type FEI Helios 600 (Dual Beam). The resolution was 0.9 nm at 15 kV at optimal working distance and 1 nm at 15 kV at the coincidence point. The images of the sample surface were generated at acceleration voltages between 0.35 and 30 kV and at working distances between 1 and 10 mm. For the detection of secondary or backscattered primary electrons an Everhart–Thornley or an in-lens detector may be used, and for STEM studies (scanning transmission electron microscopy) a bright field, dark field and 12-segment HAADF (high-angle annular dark field) detector. For cryo-SEM investigations, a Quorum PP2000T preparation-system is available. Energy dispersive X-ray analysis (EDX) measurements were performed with an Oxford X-Max80 silicon drift detector (SDD) with an ATW2-window and an energy resolution down to 129 eV. The detection angle of the detector was 35°.

Film thickness measurements were performed using a variable-angle spectroscopic ellipsometer (VASE; from J.A. Woollam Co., USA) with incident angles of 75° and 65° in the spectral range of 300–800 nm. A fit procedure based on a Cauchy model describing the plasma polymer coating was employed.

Using a light microscope (Keyence VHX500) under ambient conditions, AM50 substrates with a size of 25 × 25 mm were submitted to the hydrogen bubble formation test (H2BT), contacting the substrate surface with approximately 0.27 mL of water or aqueous polymer formulations. Videos of up to 20 min duration were recorded. Details of the procedure are described elsewhere [12].

Results and discussion

This section initially highlights some of the bulk and surface properties of the magnesium alloy AM50 substrates. After this, the characteristics of the four distinct layer systems as depicted in Fig. 2 and applied to polished AM50 surfaces will be highlighted and discussed. Finally, an outlook concerning ongoing investigations will be presented.

Characterization of polished AM50 substrates

According to the EDX characterization performed with a primary electron energy of 30 keV, the AM50 substrates under investigation were composed of 86 wt% magnesium, 5.5 wt% aluminum, 0.5 wt% zinc, 0.3 wt% manganese, and 0.1 wt% silicon, with the balance comprising carbon and oxygen containing species attributed to the sample surfaces. Figure 3 shows the results of the quantitative EDX mapping obtained with an electron acceleration voltage of 5 kV for a crosscut of a laser-treated AM50 substrate. The bottom part of the maps is indicative of the sample regions which are basically unaffected by the laser treatment and which show a grain structure with grain sizes ranging from 2 to 20 µm. The elemental concentrations of aluminum are elevated around regions with high magnesium concentrations. This finding is interpreted as an enrichment of aluminum at the grain boundaries. On the other hand, the area density of comparatively small grains with the highest aluminum and the lowest magnesium concentrations is lower than 1 %. Such grains are attributed to intermetallic phases such as the β-phase, $Mg_{17}Al_{12}$, which may be expected to be harder and nobler than the magnesium-rich α-phase [24].

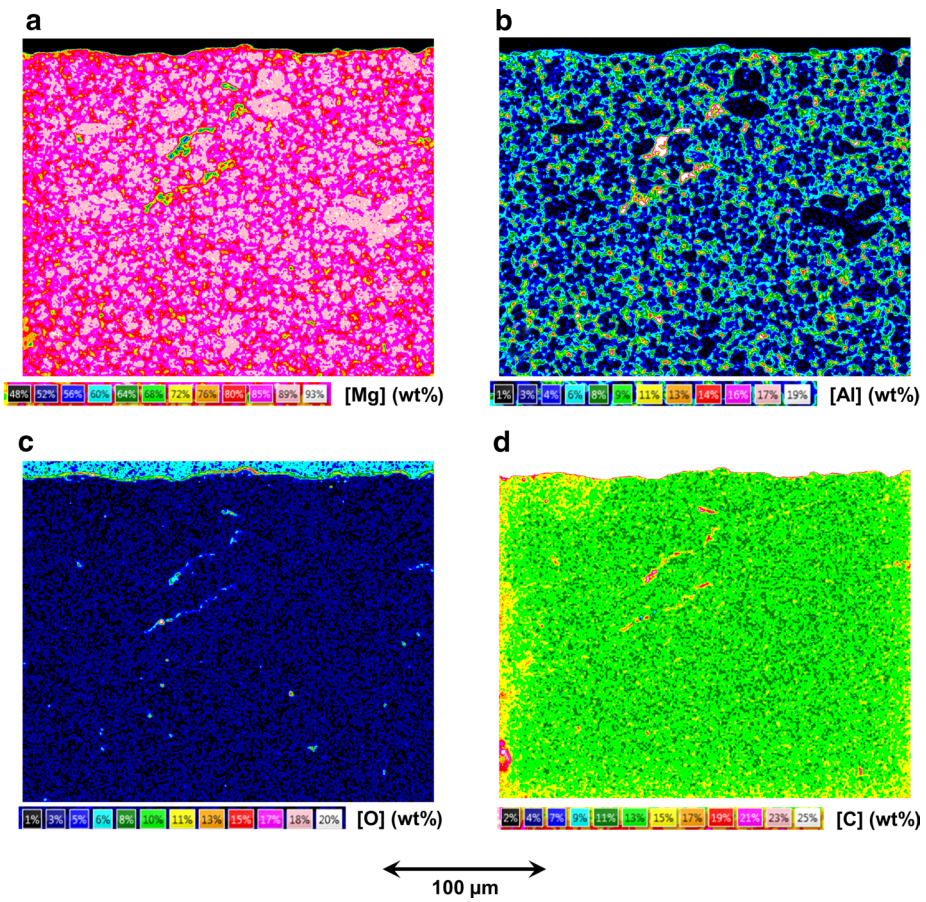

Fig. 3 EDX mapping (width 260 µm) showing a crosscut of a laser-treated AM50 substrate, with the treated surface oriented towards the *top*, in contact with an embedding compound containing filler particles. *Maps* indicating the distribution of **a** magnesium, **b** aluminum, **c** oxygen, and **d** carbon based on the respective K_α X-ray series are displayed, and the concentrations [Mg], [Al], [O], and [C] are given in weight% (wt%)

Accordingly, the lamellar grain protruding from the polished AM50 surface shown in the SFM image in Fig. 4 is interpreted to contain crystallites of intermetallic phases which have a greater resistance to the abrasive sandpaper treatment than the softer magnesium-rich surface regions. The grooves visible in the SFM image, which represent a grain surface on the polished AM50 surface in Fig. 5a within a region exhibiting a root mean square (rms) roughness of 13 nm, may result from the mechanical removal of material in line with the polishing direction. In addition, Fig. 5c presents the SFM image of an AM50 substrate immersed in water for 15 s. The respective surface area shows an rms roughness of 45 nm and does not reveal surface features oriented in a preferential direction.

These findings are attributed to the removal of several tens of nanometers of magnesium material during the 15 s contact with water. This material removal occurs concomitantly with the formation of hydrogen bubbles that was observed after 3 s of contact between the polished AM50 and liquid water, as can be seen from the respective plot in Fig. 6.

Summarizing the findings for the properties of polished AM50 substrates, one aspired functional property of a coating system on AM50 surfaces in contact with liquid water films may be the delay of the onset of hydrogen bubble formation and the lowering of the area density of surface sites contributing to the formation of hydrogen bubbles.

Characterization of coated AM50 substrates

The four distinct coating systems applied to polished AM50 surfaces will be regarded in the sequence depicted in Fig. 2.

Three $SiO_xC_yH_z$-type plasma polymer layers were deposited in a low pressure plasma batch process on polished AM50 substrate surfaces. Following VASE inspection and XPS characterization, layer thicknesses of 493, 693, or 492 nm were obtained for layers showing a low (L), medium (M) or high (H) content of (hydro)carbon species amounting to values between 7 at.% and 41 at.%. Figure 7 shows images obtained after the contact of a water aerosol on the surfaces of the respective plasma polymer layers, in the frame

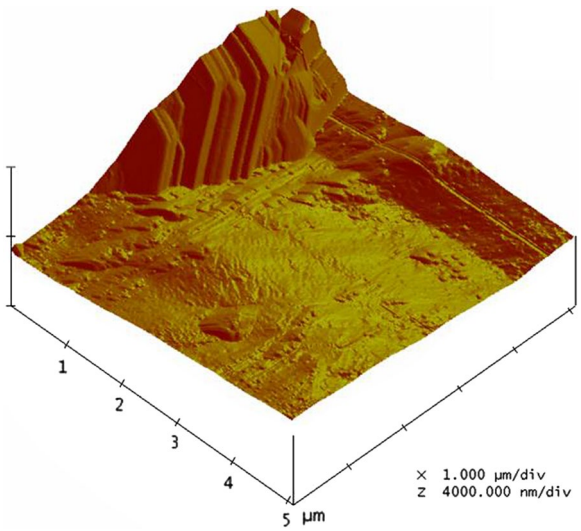

Fig. 4 SFM image of a grain protruding from a polished AM50 surface

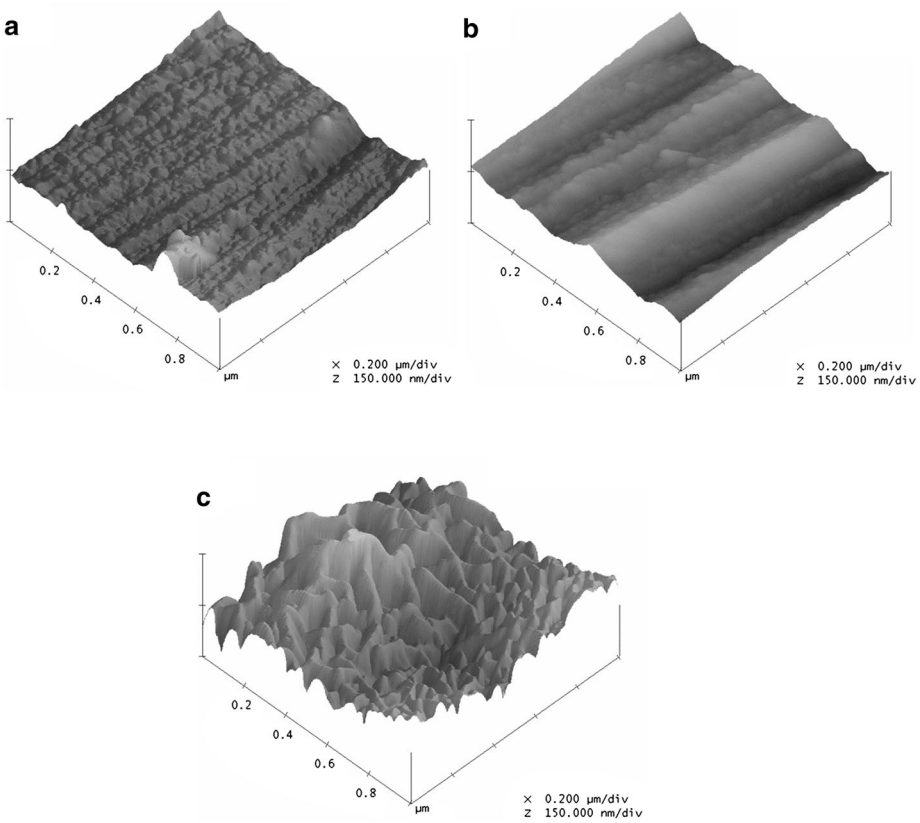

Fig. 5 SFM images of grain surfaces imaged on **a** a polished AM50 surface, **b** an AM50 surface immersed in aqueous laccase formulation for 15 s and **c** an AM50 surface immersed in water for 15 s

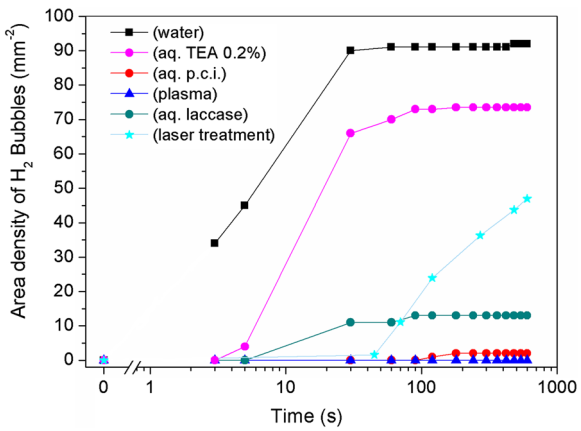

Fig. 6 Time-dependent plot showing the area density of hydrogen bubbles microscopically perceived upon contact with polished AM50 substrate surfaces with water ("water") or aqueous formulations, such as 0.2 wt% solution of triethanolamine (TEA) in water ("aq. TEA 0.2%"), 1 wt% formulation of the polymeric corrosion inhibitor (p.c.i.) G50 wb ("aq. p.c.i."), or an aqueous formulation of a biopolymer mixture containing the enzyme laccase and the polysaccharide maltodextrin ("aq. laccase"). The plasma polymer coated ("plasma") or laser treated ("laser treatment") AM50 surfaces were contacted with water

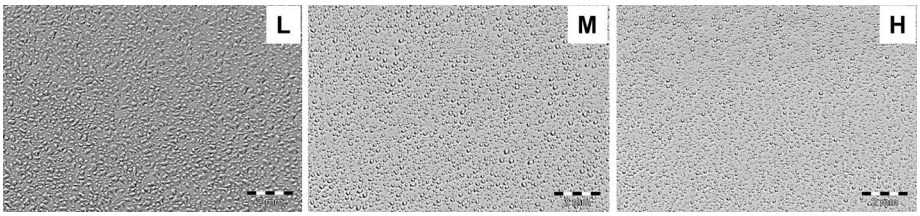

Fig. 7 Light microscopy images of AM50 substrate surfaces covered with $SiO_xC_yH_z$-type plasma polymer layers with a low (*L*), medium (*M*) or high (*H*) content of (hydro)carbon species

of an AWT. The water droplet size distribution is perceived to be homogeneous across the substrate surface, and the corresponding water contact angles measured for the L, M, and H surfaces were 47 ± 2°, 75 ± 1°, and 96 ± 5°, respectively. These wetting results indicate that an increased carbon content of the plasma polymer layers results in more hydrophobic surfaces that are characterized by a smaller average droplet size in AWT investigations. Consequently, the interaction with a liquid water film can be tuned by varying the surface composition of the plasma polymer layers. Moreover, the lateral and vertical layer homogeneity and water permeability were adjusted such that the H2BT did not reveal any hydrogen bubble formation over 20 min (cf. Fig. 6). Finally, it may be highlighted that the non-centrosymmetric structure of the investigated plasma polymer films was also due to them being based on highly crosslinked plasma polymer primer layers in contact with the AM50 substrate.

In a second approach, laser-treated AM50 surfaces were investigated. Figure 8 shows the scanning electron microscopy images obtained with a primary electron energy of 30 keV. In the case of the image taken from a polished AM50 substrate surface and shown in Fig. 8a, grooves resulting from the polishing treatment can be seen, and the material contrast resulting from the collection of back-scattered electrons is attributed to aluminum enrichment at grain boundaries around grains rich in magnesium. Following the laser treatment, the surface topography results roughened, and substantial material transport was suggested by the lack of evidence for polishing grooves, as may

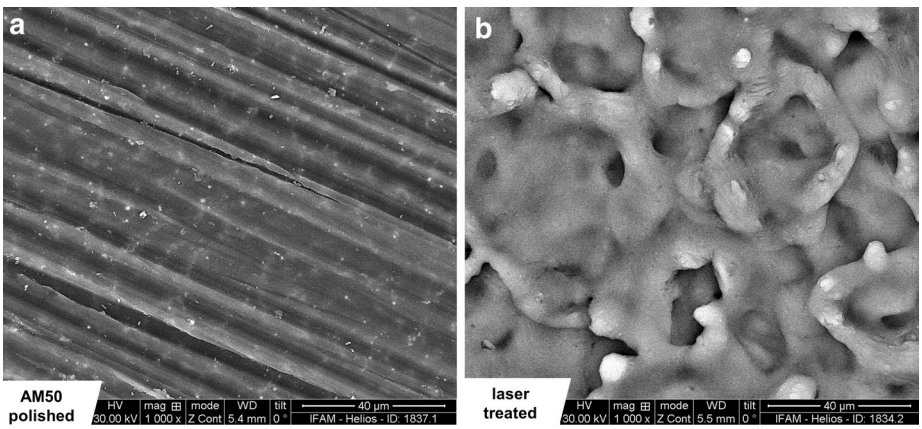

Fig. 8 SEM images obtained with a primary electron energy of 30 keV and also collecting back-scattered electrons from **a** a polished AM50 substrate surface and **b** a laser-treated AM50 surface

be inferred from Fig. 8b. Moreover, the upper regions of the EDX maps shown in Fig. 3 indicate that an uptake of oxygen containing species into the sample surface resulted from the laser treatment, with the thickness of the thus chemically modified layer amounting to some hundred nanometers. Finally, the surface of the non-centrosymmetric reaction layer can be tuned by varying, e.g., the concentrations of oxygen and carbon dioxide in the gas phase during laser treatment. Exposing pristine surfaces of light metal samples, e.g. aluminum, to gas mixtures containing O_2 and CO_2 has been shown to result in the formation of reaction layers with different thickness and composition as compared to exposure in pure O_2 or CO_2 at room temperature [25]. The formation of carbonate-based surface groups can be inferred from the XPS investigations comparing a laser-treated AM50 surface to a polished surface. Figure 9 displays survey spectra (Fig. 9d) and the detail photoelectron emissions obtained for the C 1s (Fig. 9a), O 1s (Fig. 9b), and Mg 2p. (Fig. 9c) regions when investigating a polished AM50 surface or a laser-treated surface. In detail, the C1 s spectra showed signal contributions centered at 285.0 ± 0.1, 286.2 ± 0.2, 287.8 ± 0.1, 289.2 ± 0.2, and 290.4 ± 0.2 eV which are attributed to hydrocarbonaceous carbon, C*–O, C*= O, and carboxylic or carbonate species, respectively [25–28]. The C1s spectra revealed the formation of highly oxidized carbon species with binding energies higher than 289 eV, based on a carbon surface concentration around 25 at.%. The O 1s spectra showed signal contributions centered at 530.0 ± 0.2 and 532.0 ± 0.2 eV which are attributed to oxide and hydroxide or carbonate

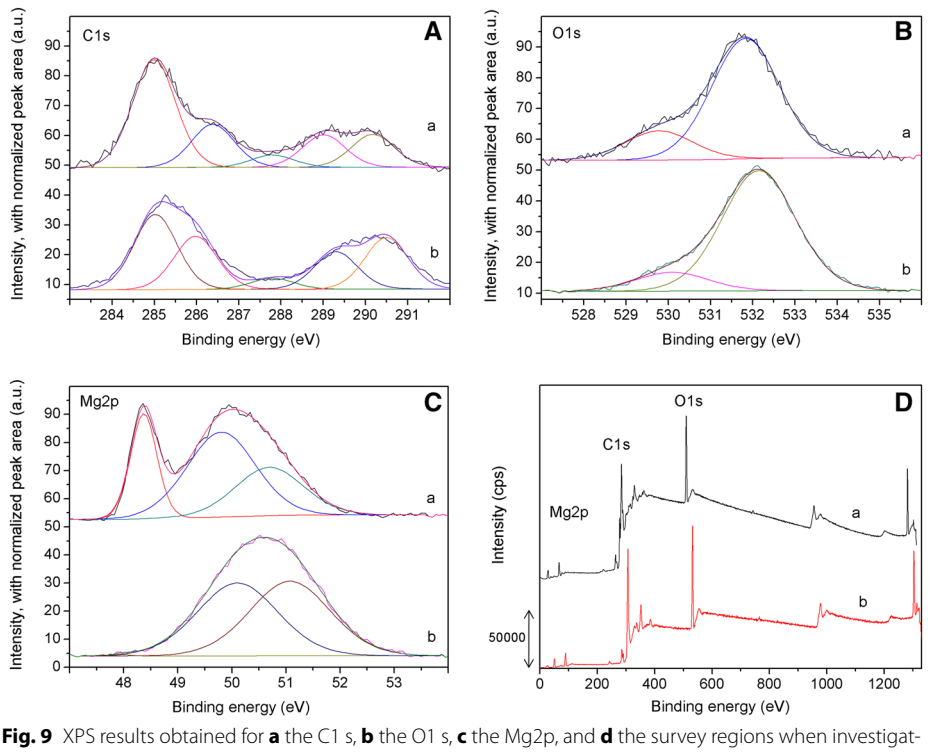

Fig. 9 XPS results obtained for **a** the C1 s, **b** the O1 s, **c** the Mg2p, and **d** the survey regions when investigating a polished AM50 surface (**a**) or a laser-treated surface (**b**). The intensities for the detail plots **a**, **b**, and **c** are normalized with reference to the respective total signal area

species, respectively [27, 29]. Finally, the Mg 2p spectra showed signal contributions centered at 48.4 ± 0.1 eV (only in the case of the polished AM50 surface), 50.0 ± 0.2, and 50.9 ± 0.2 eV which are attributed to metallic magnesium, magnesium oxide and magnesium hydroxide or carbonate species, respectively [27, 29]. The Mg 2p spectra reveal the formation of a more than 10 nm thick reaction layer comprising oxidized magnesium species as a consequence of the laser treatment.

As presented in Fig. 6, laser-treated AM50 substrates showed strongly delayed hydrogen bubble formation upon contact with liquid water as compared to the polished samples. In addition, XPS investigations performed with a variation in the time of contact between a polished AM50 surface or a laser-treated surface and a water film revealed that the increase in the [Al]/[Mg] surface concentration ratio was strongly delayed in the case of the laser-treated surfaces (cf. Fig. 10). This shows that the dynamics of the interaction between a water film and an AM50 substrate can be tuned by the formation of a sub-microscopic reaction layer using laser treatment.

An even stronger delay in hydrogen bubble formation can be achieved by applying an aqueous formulation of a layer-forming polymeric corrosion inhibitor (p.c.i.), namely G50 wb, to a polished AM50 surface [12]. As revealed by the results presented in Fig. 6, this effect resulted from the polymer additive G50. It is clear that adding 0.2 wt% TEA to water to adjust a slightly alkaline pH value of around 8 only marginally affects the onset of hydrogen bubble formation or the area density of hydrogen bubbles observed after 30 s. Following the results displayed in Fig. 11, lowering the polymer concentration in the formulation in contact with the polished AM50 surface resulted in an increased hydrogen bubble density, as observed after 20 min of immersion. This effect became more pronounced as soon as a minimum concentration of around 0.5 wt% was no longer maintained. A non-centrosymmetric polymer layer structure was suggested based on dissipative particle dynamics (DPD) simulations [12], and a polymer adsorbate effective in delaying the interaction between the AM50 surface and a liquid water film appeared to be preferentially formed when the polymer solubility in the aqueous formulation was exceeded. Such behavior may be expected for the adsorption of amphiphilic molecules.

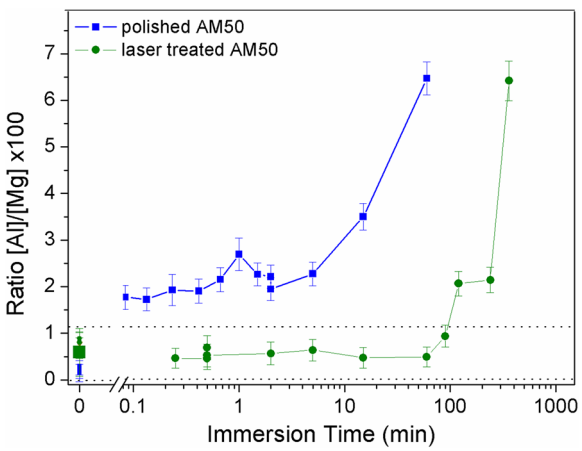

Fig. 10 XPS results obtained for the [Al]/[Mg] surface concentration ratio when varying the time of contact between a polished AM50 surface or a laser-treated surface and a water film

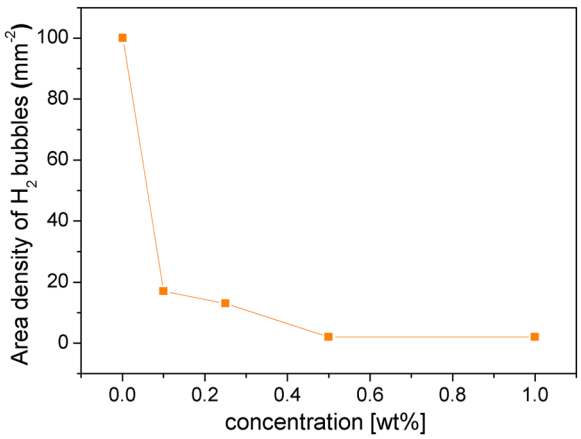

Fig. 11 Hydrogen bubble formation test results obtained when varying the concentration of an aqueous formulation of polymeric corrosion inhibitor (G50 wb) in contact with a polished AM50 surface for 20 min

With the resistance of the resulting polymer films to rinsing with water, they seem to be promising candidates for application not only as surfactants but also as interfactants, should further films be intended to be grown on top of a polymer-coated surface. Unlike surfactants which are active at the surface of (multi)layer systems, the concept of interfactants was introduced for layers which are more strongly bound to the substrate than the film to be grown [30], and which affect the kinetics of the subsequently growing molecular layers. Interfactant layers are generally discussed in the context of growth occurring from species adsorbed from the gas phase, and they may form wetting layers separating molecular films from a substrate [31] and constituting a diffusion barrier [32]. Moieties forming interfactant layers can be atomic, molecular or ionic species, and the concept could be extended to strongly adsorbed polymeric species affecting the growth of subsequent molecular layers from a condensed phase.

Finally, such an approach may also be applied for adsorbates formed from patchy globular polypeptide nanoparticles such as the hydrated enzyme laccase. Layers on silica surfaces obtained from aqueous mixtures with maltodextrin at a pH value of 4.8 have recently been shown to be resistant to rinsing with water [13]. With respect to the interaction between polished AM50 surfaces and aqueous suspensions containing laccase and maltodextrin at neutral pH values, the Hydrogen Bubble Formation Test indicated a fast formation of adsorbates that delayed the onset of hydrogen bubble formation, as shown in Fig. 6. Moreover, the results of the SPM investigations displayed in Fig. 5 indicate that after the immersion of polished AM50 substrates for 15 s (Fig. 5b), grooves resulting from polishing could still be perceived, and that an rms roughness of 12 nm was obtained. The surface morphology was similar to that of polished AM50 (Fig. 5a) and clearly distinct from that obtained for AM50 substrates immersed in water for 15 s (Fig. 5c). Thus, the biopolymer mixture adsorbs fast enough to affect the onset of hydrogen bubble formation upon reaction of the inhomogeneous surface of the magnesium alloy with water. The results of the XPS investigations obtained for films on AM50 substrates are shown in Table 1. These indicate the detection of nitrogen containing species characteristic of laccase following contact of AM50 with aqueous biopolymer formulations containing

Table 1 Results of XPS investigations, with surface concentrations given in atomic % (at%), performed for polished AM50 samples and AM50 substrates in contact for distinct periods with aqueous (aq.) biopolymer formulations containing laccase and maltodextrin

Sample	[N] (at.%)	$[C]^{total}$ (at.%)	$[C^*–O]/[C]^{total}$	$[Mg]^{total}$ (at.%)	$[Mg^0]/[Mg]^{total}$
AM50, polished	–	29.1	0.18	23.5	0.23
AM50, 15 s immersion in aq. laccase	1.9	31.2	0.25	25.8	0.24
AM50, 60 s immersion in aq. laccase	1.5	33.4	0.26	18.0	–
AM50, 30 min immersion in aq. laccase	2.6	40.1	0.34	13.8	–

laccase and maltodextrin for distinct periods, while species containing oxygen-bonded carbon atoms C*–O contained in maltodextrin were found on non-rinsed samples.

In summary, four approaches are depicted in Fig. 2. Cases a and b comprise dry processes with reactive precursors and a physical energy impact. Cases c and d comprise wet processes and are based on adsorption at room temperature. These approaches may be compared with respect to their effectivity in delaying the onset of hydrogen bubble formation in water films that are in contact with magnesium alloy surfaces, as illustrated in Fig. 6. Concerning the approaches based on dry processes, layer systems with a thickness of between 0.1 and 1 µm have been presented. Closed, dense and smooth, and integrally applied $SiO_xC_yH_z$-type plasma polymer layers deposited in low pressure plasma showed superior effectivity compared to reaction layers formed locally by laser treatment in air. Tuning the composition of the gas phase and further optimizing the parameters guiding the energy impact during the laser treatment will contribute to increasing the performance of these layers. In comparison with PECVD or high-energy laser [22] processes the application of liquid formulations by dipping or spraying facilitates a less elaborate or milder surface functionalization, resulting in thinner layers allowing for instance the modification of nanostructured substrates [33, 34]. Concerning the approaches based on wet processes, the investigated natural biopolymer mixtures containing laccase and maltodextrin, as well as the synthetic amphiphilic polymers optimized for the application on aluminum alloys [35], showed multi-metal effectivity evidenced by a fast adsorption on AM50 surfaces, resulting in layers with a thickness between 0.001 and 0.01 µm. Using an aqueous G50 wb formulation revealed superior performance in suppressing the formation of hydrogen bubbles for time ranges of up to 20 min. That is a time-scale comparable to that required for the drying and hardening of water-based primer, coating or adhesive systems. Combining such approaches with the application of a preceding dry process, as shown for cases a and b, may further enhance the performance of the functional layer system.

Conclusions

In this contribution, the effects of barrier layers, which had been applied to polished magnesium alloy AM50 surfaces either by the deposition of siliceous polymer coatings in low pressure plasma processes, by laser surface treatments in controlled gas atmospheres, or by dipping in liquid formulations containing a recently developed polymeric inhibitor or a mixture of the enzyme laccase and the polysaccharide maltodextrin, were monitored with regards to their interactions with molecular water films. These films

may be comprehended as a simplified implementation of mixed molecular films that are essential during the build-up of adhesion in painting or adhesive systems. For this purpose, we described the design of layer systems composed of single, non-centrosymmetric layers deposited using process materials and protocols that can be applied to various substrates. Combinations of the layer-forming processes presented may result in an even more effective multilayer-functionalization of magnesium substrates.

Authors' contributions

StSt and PSt laid out and performed the Hydrogen Bubble Formation Test, contributed to the discussion of microscopic and spectroscopic data; PSt and WN also contributed with the AM50 laser surface treatment; YC performed Scanning Probe Microscopy investigations and developed and set up the biofunctionalization experiments of magnesium surfaces with laccase supported by StSt and contributed to the lay-out and formatting of the article; DS trained and advised the low pressure plasma team comprising GH and WK who performed the plasma polymer coatings and characterized their structural and surface properties; JI trained and advised the laser surface treatment team comprising PSt and WN who contributed to the laser treatment and the microscopic and spectroscopic characterization of the surfaces; MN trained and advised the surface characterization team, comprising StSt, PSt and WN, and took part in defining and setting up the experiments, performing XPS investigations, and analyzing data; and WLC contributed in planning the conceptual approach for joint research in several teams, discussing and merging the obtained data, and in drafting the manuscript. All authors read and approved the final manuscript.

Authors' information

StSt, PSt, GH, WN, and WK participated in the program Science without Borders at Fraunhofer IFAM Bremen, where the experiments were performed.

Author details

[1] Department of Adhesive Bonding Technology and Surfaces, Fraunhofer Institute for Manufacturing Technology and Advanced Materials IFAM, Wiener Straße 12, 28359 Bremen, Germany. [2] Department of Chemistry, Federal University of Santa Catarina (UFSC), Campus Universitário Trindade, Florianópolis, SC 8040-900, Brazil. [3] Department of Materials, UEPG, State University of Ponta Grossa, Avenida de General Carlos Cavalcanti 4748, Ponta Grossa, PR, Brazil. [4] Programa de Pós-Graduação em Ciência e Tecnologia de Materiais (POSMAT), São Paulo State University (UNESP), Av. Eng. Luiz Edmundo Carrijo Coube 14-01, Bauru, São Paulo 17033-360, Brazil. [5] National Nanotechnology Laboratory LANOTEC, Centro Nacional de Alta Tecnología, 1.3 km, Norte de la Embajda de EE.UU. Pavas, San José, Costa Rica.

Acknowledgements

The authors are grateful to Science without Borders (Ciência sem Fronteiras), to Conselho Nacional de Desenvolvimento Científico e Tecnológico (CNPq) (Science without Borders Process N 238488/2012-8 Priscilla Stachera from September 2012 to August 2013, 203099/2011-7 Wilson Neto from March 2012 to February 2013, 203078/2011-0 Gustavo Hrycyna from March 2012 to February 2013, 238434/2012-5 Wagner Kazuki de Azambuja from March 2012 to February 2013) and to Coordenação de Aperfeiçoamento de Pessoal de Nível Superior (CAPES) (Science without Borders Process N 88888.020610-2013-00 Stephani Stamboroski from September 2013 to December 2014), to CONICIT Costa Rica, to Leandro Gonçalves de Andrade Rosato for support when applying the Aerosol Wetting Test (AWT), Dr. Marko Soltau for providing material and taking part in fruitful discussions, to Dr. Karsten Thiel for performing electron microscopy investigations, to Dr. Uwe Specht for facilitating laser surface treatments, and to Prof. Dr. João Carlos Gomes and, last but not least, to Prof. Dr. Bernd Mayer for their steady support.

Competing interests

The authors declare that they have no competing interests.

Received: 15 January 2016 Accepted: 16 April 2016
Published online: 09 May 2016

References

1. Mordike BL, Ebert T. Magnesium Properties—applications—potential. Mat Sci Eng A. 2001;302:37–45. doi:10.1016/S0921-5093(00)01351-4.
2. Zeng RC, Zhang J, Huang WJ, Dietzel W, Kainer KU, Blawert C, Ke W. Review of studies on corrosion of magnesium alloys. Trans Nonferrous Metals Soc China. 2006;16:s763–71. doi:10.1016/S1003-6326(06)60297-5.
3. Gray JE, Luan B. Protective coatings on magnesium and its alloys—a critical review. J Alloys Compd. 2002;336:88–113. doi:10.1016/S0925-8388(01)01899-0.
4. Witte F. The history of biodegradable magnesium implants: a review. Acta Biomater. 2010;6:1680–92. doi:10.1016/j.actbio.2010.02.028.
5. Li N, Zheng Y. Novel magnesium alloys developed for biomedical application: a review. J Mater Sci Technol. 2013;29:489–502. doi:10.1016/j.jmst.2013.02.005.
6. Scharf S, Noeske M, Cavalcanti WL, Schiffels P. Multi-functional, self-healing coatings for corrosion protection: materials, design and processing. In: Makhlouf ASH editor. Handbook of Smart Coatings for Materials Protection. Cambridge: Woodhead Publishing. 2014. doi: 10.1533/9780857096883.1.75.

7. Stenzel V, Rehfeld N. Functional coatings. European coatings tech files. Hanover: Vincentz Network; 2011.
8. Hartwig A, Meissner R, Merten C, Schiffels P, Wand P, Grunwald I. Mutual influence between adhesion and molecular conformation: molecular geometry is a key issue in interphase formation. J Adhes. 2013;89:77–95. doi:10.1080/00218464.2013.731363.
9. Cavalcanti WL, Noeske PLM. Investigating dynamic interactions by multi-scale modelling: from theory to applications. Chem Modell. 2014;11:175–200. doi:10.1039/9781782620112-00175.
10. Meilikhov M, Furukawa S, Hirai K, Fischer RA, Kitagawa S. Binary janus porous coordination polymer coatings for sensor devices with tunable analyte affinity. Angew Chem. 2013;125:359–63. doi:10.1002/ange.201207320.
11. Du J, O'Reilly RK. Anisotropic particles with patchy, multicompartment and Janus architectures: preparation and application. Chem Soc Rev. 2011;40:2402–16. doi:10.1039/C0CS00216J.
12. Gonçalves LMG, Sanchez LC, Stamboroski S, Urena YRC, Cavalcanti WL, Ihde J, Noeske M, Soltau M, Brune K. Instantly investigating the adsorption of polymeric corrosion inhibitors on magnesium alloys by surface analysis under ambient conditions. J Surf Eng Mat Adv Technol. 2014;4:282–94. doi:10.4236/jsemat.2014.45032.
13. Ureña YRC, Gaetjen L, Nascimento MV, Noeske PLM, Lisboa Filho PN, Cavalcanti WL, Rischka K. Investigations of biofilms formed on silica substrates in contact with aqueous formulations containing laccase and maltodextrin. Appl Adhes Sci. 2016;4:2. doi:10.1186/s40563-016-0059-3.
14. Huang L, Yi J, Gao Q, Wang X, Chen Y, Liu P. Carboxymethyl chitosan functionalization of CPED-treated magnesium alloy via polydopamine as intermediate layer. Surf Coat Technol. 2014;258:664–71. doi:10.1016/j.surfcoat.2014.08.020.
15. Zhen Z, Xi TF, Zheng YF. Surface modification by natural biopolymer coatings on magnesium alloys for biomedical applications. In: Narayanan TSNS, Park IS, Lee MH editors. Surface Modification of Magnesium and its alloys for biomedical applications. Cambridge: Woodhead Publishing. 2015. doi: 10.1016/B978-1-78242-078-1.00011-6.
16. Salz D, Vissing KD. Scratch-resistant and expandable corrosion prevention layer for light metal substrates. US Patent 20120003483 A1. 5 Jan 2012.
17. Lommatzsch U, Ihde J. Plasma polymerization of HMDSO with an atmospheric pressure plasma jet for corrosion protection of aluminum and low-adhesion surfaces. Plasma Process Polym. 2009;6:642–8. doi:10.1002/ppap.200900032.
18. Noeske M, Thiel K, Burchardt M, Specht U, Lukasczyk T, Ihde J. Laser-Prozess zur Erzeugung von Beschichtungen auf Leichtmetall (legierungen) sowie resultierende Beschichtungen und Produkte. DE 10 2013210176 B3, 25 Sept 2014.
19. Ishizaki T, Hieda J, Saito N, Saito N, Takai O. Corrosion resistance and chemical stability of super-hydrophobic film deposited on magnesium alloy AZ31 by microwave plasma-enhanced chemical vapor deposition. Electrochim Acta. 2010;55:7094–101. doi:10.1016/j.electacta.2010.06.064.
20. Kuo YL, Chang KH. Atmospheric pressure plasma enhanced chemical vapor deposition of SiO_x films for improved corrosion resistant properties of AZ31 magnesium alloys. Surf Coat Technol. 2015;283:194–200. doi:10.1016/j.surfcoat.2015.11.004.
21. Zimmermann S, Specht U, Spieß L, Romanus H, Krischok S, Himmerlich M, Ihde J. Improved adhesion at titanium surfaces via laser-induced surface oxidation and roughening. Mat Sci Eng A. 2012;558:755–60. doi:10.1016/j.msea.2012.08.101.
22. Schneider N, Wrobel C, Holtmannspötter J. Use of high-energy laser radiation for surface preparation of magnesium for adhesive applications. Appl Adhes Sci. 2015;4:1. doi:10.1186/s40563-016-0058-4.
23. Brune K, Tornow C, Noeske M, Wiesner T, Barbosa AFQ, Stamboroski S, Dieckhoff S, Mayer B. Surface analytical approaches contributing to quality assurance during manufacture of functional interfaces. Appl Adhes Sci. 2015;3:2. doi:10.1186/s40563-014-0030-0.
24. Song G, Atrens A. Understanding magnesium corrosion—a framework for improved alloy performance. Adv Eng Mat. 2003;5:837–58. doi:10.1002/adem.200310405.
25. Tornow C, Noeske PLM, Dieckhoff S, Wilken R, Gärtner K. Preparation and characterization of carbonate terminated polycrystalline Al_2O_3/Al films. Appl Surf Sci. 2005;252:1959–65. doi:10.1016/j.apsusc.2005.03.176.
26. Peng XD, Barteau MA. Spectroscopic characterization of surface species derived from HCOOH, CH_3COOH, CH_3OH, C_2H_5OH, $HCOOCH_3$, and C_2H_2 on MgO thin film surfaces. Surf Sci. 1989;224:327–47. doi:10.1016/0039-6028(89)90918-7.
27. Feliu S Jr, Merino MC, Arrabal R, Coy AE, Matykina E. XPS study of the effect of aluminium on the atmospheric corrosion of the AZ31magnesium alloy. Surf Interfac Anal. 2009;41:143–50. doi:10.1002/sia.3004.
28. Wei Q, Krysiak S, Achazi K, Becherer T, Noeske PLM, Paulus F, Liebe H, Grunwald I, Dernedde J, Hartwig A, Hugel T, Haag R. Multivalent anchored and crosslinked hyperbranched polyglycerolmonolayers as antifouling coating for titanium oxide surfaces. Colloids Surf B: Biointerfac. 2014;122:684–92. doi:10.1016/j.colsurfb.2014.08.001.
29. Ghijsen J, Namba H, Thiry PA, Pireaux JJ, Caudano P. Adsorption of oxygen on the magnesium (0001) surface studied by XPS. Appl Surf Sci. 1981;8:397–411. doi:10.1016/0378-5963(81)90094-5.
30. Schmidt T, Bauer E. Interfactant-mediated quasi-Frank–van der Merwe growth of Pb on Si(111). Phys Rev B. 2000;62:15815–25. doi:10.1103/PhysRevB.62.15815
31. Kury P, Roos KR, Thien D, Möllenbeck S, Wall D, Horn-von Hoegen M, Meyer zu Heringdorf FJ. Disorder-mediated ordering by self-interfactant effect in organic thin film growth of pentacene on silicon. Organ Electron. 2008;9:461–5. doi:10.1016/j.orgel.2008.02.006.
32. Ketteler G, Ranke W, Schlögl R. An interfactant for metal oxide heteroepitaxy: growth of dispersed ZrO_2(111) films on FeO(111) precovered Ru(0001). Phys Chem Chem Phys. 2004;6:205–8. doi:10.1039/b314077f.
33. Cui Z, Yin L, Wang Q, Ding J, Chen Q. A facile dip-coating process for preparing highly durable superhydrophobic surface with multi-scale structures on paint films. J Coll Interfac Sci. 2009;337:531–7. doi:10.1016/j.jcis.2009.05.061.
34. Corrales Ureña YR, Wittig L, Vieira Nascimento M, Faccioni JL, Noronha Lisboa Filho P, Rischka K. Influences of the pH on the adsorption properties of an antimicrobial peptide on titanium surfaces. Appl Adhes Sci. 2015;3:7. doi:10.1186/s40563-015-0032-6.
35. Cavalcanti W, Buchbach S, Soltau M. Anticorrosive systems—dual-purpose defenders. Eur Coat J. 2012;10:30–3.